The $\alpha_2\delta$ subunits of voltage-gated calcium channels form GPI-anchored proteins, a posttranslational modification essential for function

Anthony Davies[1], Ivan Kadurin[1], Anita Alvarez-Laviada[1], Leon Douglas, Manuela Nieto-Rostro, Claudia S. Bauer, Wendy S. Pratt, and Annette C. Dolphin[2]

Department of Neuroscience, Physiology and Pharmacology, University College, London WC1E 6BT, United Kingdom

Edited by William A. Catterall, Department of Pharmacology, University of Washington, Seattle, and accepted by the Editorial Board November 30, 2009 (received for review August 3, 2009)

Voltage-gated calcium channels are thought to exist in the plasma membrane as heteromeric proteins, in which the α1 subunit is associated with two auxiliary subunits, the intracellular β subunit and the $\alpha_2\delta$ subunit; both of these subunits influence the trafficking and properties of Ca_V1 and Ca_V2 channels. The $\alpha_2\delta$ subunits have been described as type I transmembrane proteins, because they have an N-terminal signal peptide and a C-terminal hydrophobic and potentially transmembrane region. However, because they have very short C-terminal cytoplasmic domains, we hypothesized that the $\alpha_2\delta$ proteins might be associated with the plasma membrane through a glycosylphosphatidylinositol (GPI) anchor attached to δ rather than a transmembrane domain. Here, we provide biochemical, immunocytochemical, and mutational evidence to show that all of the $\alpha_2\delta$ subunits studied, $\alpha_2\delta$-1, $\alpha_2\delta$-2, and $\alpha_2\delta$-3, show all of the properties expected of GPI-anchored proteins, both when heterologously expressed and in native tissues. They are substrates for prokaryotic phosphatidylinositol-phospholipase C (PI-PLC) and trypanosomal GPI-PLC, which release the $\alpha_2\delta$ proteins from membranes and intact cells and expose a cross-reacting determinant epitope. PI-PLC does not affect control transmembrane or membrane-associated proteins. Furthermore, mutation of the predicted GPI-anchor sites markedly reduced plasma membrane and detergent-resistant membrane localization of $\alpha_2\delta$ subunits. We also show that GPI anchoring of $\alpha_2\delta$ subunits is necessary for their function to enhance calcium currents, and PI-PLC treatment only reduces calcium current density when $\alpha_2\delta$ subunits are coexpressed. In conclusion, this study redefines our understanding of $\alpha_2\delta$ subunits, both in terms of their role in calcium-channel function and other roles in synaptogenesis.

lipid raft | posttranslational | electrophysiology | immunocytochemistry

Voltage-gated (Ca_V) calcium channels of the Ca_V1 and Ca_V2 classes are thought to exist as heteromeric complexes. These consist of an α1 subunit that forms the pore and determines the main functional and pharmacological attributes of the channel (1-3), which is associated with an intracellular-β subunit and an $\alpha_2\delta$ subunit, both of which influence the trafficking of the channels and their kinetic and voltage-dependent properties. The molecular characterization and topology of the $\alpha_2\delta$ subunits were initially determined for skeletal muscle $\alpha_2\delta$-1 (4-8), but they have been suggested to generalize to all four characterized $\alpha_2\delta$ subunits (for review, see ref. 9). When $\alpha_2\delta$-1 was purified from skeletal muscle, it was identified that the extracellular α_2 subunit is bonded by disulfide to a δ subunit (5, 6). Both subunits are the product of a single gene encoding the $\alpha_2\delta$ protein, which is then posttranslationally cleaved (4). The $\alpha_2\delta$ subunits are universally described as type-I transmembrane proteins, because they have an N-terminal signal peptide and a C-terminal hydrophobic and potentially transmembrane region. The α_2 moiety was found to play a role in enhancement of calcium currents, whereas the δ subunit modified the voltage-dependent properties (8, 10).

We noted that all of the $\alpha_2\delta$ subunits have either a very short or nonexistent C-terminal cytoplasmic domain (11). Some of the $\alpha_2\delta$ subunits have a C-terminal hydrophobic domain that is predicted to be rather short for a plasma membrane-spanning α-helix (11), which also contains helix-breaking prolines (e.g., $\alpha_2\delta$-3; Fig. 1*A*). For these reasons, we tested the hypothesis that some or all $\alpha_2\delta$ proteins might be associated with the plasma membrane through a glycosylphosphatidylinositol (GPI) anchor (ω) attached to δ, rather than a transmembrane domain. Indeed, the features outlined above, among others, cause prediction programs (12) to indicate a high probability, particularly for $\alpha_2\delta$-3, that it is a substrate for GPI anchoring (Fig. 1*A*). This process occurs within the endoplasmic reticulum, and it involves cleavage of the C-terminal hydrophobic peptide at the ω-residue (Fig. 1*A*) and attachment of a GPI group to this residue, which then attaches the protein to the membrane through its lipid side chains (13).

Results

Biochemical and Functional Evidence that $\alpha_2\delta$-3 Is Anchored by GPI. To determine whether or not $\alpha_2\delta$ subunits may be anchored by GPI, we initially focused on $\alpha_2\delta$-3 because of the strong prediction that this is the case. It is a well-established fact that GPI-modified proteins partition into Triton X-100-insoluble cholesterol-rich microdomains, also termed detergent-resistant membranes (DRMs) (13). We found that heterologously expressed $\alpha_2\delta$-3 was concentrated in DRMs (Fig. 1*B*). Both free α_2-3 and δ-3 were detected as well as full-length $\alpha_2\delta$-3 (Fig. S1), indicating that the protein is incompletely proteolytically cleaved after heterologous expression, which is the case for all $\alpha_2\delta$ subunits (14).

The $\alpha_2\delta$-3 in DRMs was then treated with prokaryotic phosphatidylinositol-phospholipase C (PI-PLC), which cleaves GPI anchors. After cleavage, many GPI-anchored proteins, such as prion proteins, showed a characteristic increase in apparent molecular weight (MW) because of the anomalous interaction of the GPI anchor with SDS (13). This was observed for δ-3 after PI-PLC treatment, both before and, more clearly, after deglycosylation of the protein (Fig. 1*C*). We also found a reduction in the immunoreactivity of deglycosylated δ-3, which is a common occurrence after delipidation of GPI-anchored proteins (15, 16); it is thought to be indicative of a large conformational change in the protein between the soluble and GPI-anchored forms (as seen also in Fig. 1*E*) (17).

Author contributions: A.D., I.K., A.A.-L., L.D., M.N.-R., C.S.B., and A.C.D. designed research; A.D., I.K., A.A.-L., L.D., M.N.-R., C.S.B., W.S.P., and A.C.D. performed research; W.S.P. contributed new reagents/analytic tools; A.D., I.K., A.A.-L., L.D., M.N.-R., C.S.B., and A.C.D. analyzed data; and A.D., I.K., and A.C.D. wrote the paper.

The authors declare no conflict of interest.

This article is a PNAS Direct Submission. W.A.C. is a guest editor invited by the Editorial Board.

Freely available online through the PNAS open access option.

[1]A.D., I.K., and A.A.-L. contributed equally to this work.

[2]To whom correspondence should be addressed. E-mail: a.dolphin@ucl.ac.uk.

This article contains supporting information online at www.pnas.org/cgi/content/full/0908735107/DCSupplemental.

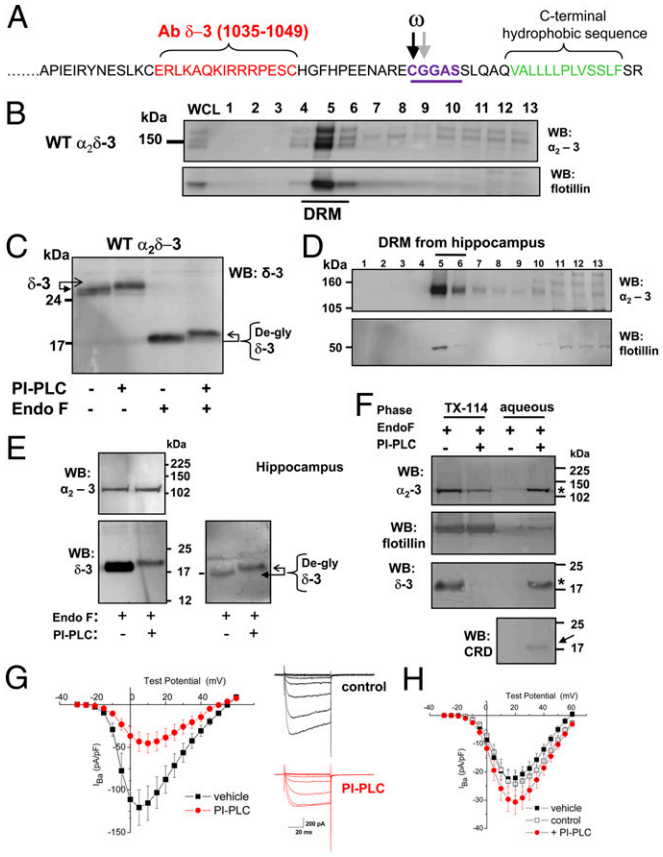

Fig. 1. Evidence that $\alpha_2\delta$-3 is GPI-anchored. (*A*) Amino acid sequence of rat $\alpha_2\delta$-3 C terminus showing the peptide used to generate the δ-3 (1035-1049) Ab in red, the two predicted GPI-anchor sites (potential ω amino acids arrowed and underlined in purple), and the C-terminal hydrophobic sequence (green). (*B Upper*) Immunoblot profile of WT $\alpha_2\delta$-3 in lipid-raft fractions (DRM) from transfected tsA-201 cells using α_2-3 (71–90) Ab. (*Lower*) Flotillin distribution in the same DRM profile. (*C*) Immunoblot of heterologously expressed $\alpha_2\delta$-3 in DRM fraction five, before and after incubation with PI-PLC and subsequent deglycosylation with endoglycosidase F (EndoF) as indicated. Deglycosylation was performed, because it enables accurate assessment of the protein MW and generally enhances immunoreactivity of the anti-peptide Abs. The Ab used was anti-δ-3 (1035-1049). The arrows show the upward shift of the δ-3 protein after PI-PLC. Similar results were obtained with PI-PLC from three different commercial sources. (*D*) Immunoblot profile of hippocampal $\alpha_2\delta$-3 with α_2-3 (71-90) Ab (*Top*) and flotillin (*Bottom*) in DRM fractions. (*E*) Hippocampal $\alpha_2\delta$-3 in DRM fraction five after deglycosylation with EndoF before and after PI-PLC as indicated. (*Top*) Immunoblot with α_2-3 Ab; (*Bottom*) immunoblot with δ-3 Ab. (*Left*) Equal loading of both lanes (25 μg protein); (*Right*) 8 μg protein in left lane and 20 μg in right lane to better compare the upward mobility shift after PI-PLC treatment, which is indicated by arrows. (*F*) PI-PLC-treated material from hippocampal DRM fraction five was subjected to phase separation in Triton X-114. This procedure is used to identify GPI-anchored proteins. The intact, amphipathic protein remains in the detergent-rich phase, whereas the PI-PLC-cleaved hydrophilic form is found in the detergent-poor (aqueous) phase (asterisk; see *SI Materials and Methods* (13). Western blots were performed on the detergent and aqueous phases to identify the presence of the different proteins. (*Top*) α_2-3. (*Middle*) Flotillin. (*Bottom*) δ-3 showing protein in the detergent (left two lanes) and aqueous phases (right two lanes) with and without PI-PLC treatment as indicated. The α_2-3 and δ-3 are indicated by an asterisk in the aqueous phase. Below this is shown a parallel blot that was probed with the CRD Ab, which shows a band at the level of δ-3 in the aqueous phase that was only observed after PI-PLC treatment (arrow). (*G Left*) Mean *I-V* relationship for $Ca_V2.2/\beta1b$ coexpressed with $\alpha_2\delta$-3 in tsA-201 cells and treated for 90 min with vehicle (■; $n = 5$) or with PI-PLC (4 U/mL; red ●; $n = 11$). (*Right*) Representative I_{Ba} currents (steps from −30 mV to +15 mV from a holding potential of −90 mV) are shown for the vehicle-treated control (black traces, *Upper*) and PI-PLC-treated (red traces, *Lower*) conditions; 1 mM Ba^{2+} was used as charge carrier. (*H*) Mean *I-V* relationship for $Ca_V2.2/\beta1b$ expressed without $\alpha_2\delta$ in tsA-201 cells and treated for 90 min with a vehicle control (■; $n = 11$), a control in which the same amount of water was added (□; $n = 20$), or a control with PI-PLC (4 U/mL; red ●; $n = 28$). No significant differences were observed under any of the conditions. Note that 5 mM Ba^{2+} was used as the charge carrier, because the currents were very small in 1 mM Ba^{2+}.

As an important confirmation, we found that native $\alpha_2\delta$-3 behaved similarly, being concentrated in DRMs from the hippocampus (Fig. 1*D*), with δ-3 showing an upward shift in mobility after PI-PLC treatment (Fig. 1*E*). PI-PLC treatment of hippocampal lysates also reduced the association of both the α_2 and δ moieties of $\alpha_2\delta$-3 with DRMs by more than 4-fold, whereas there was no effect on the localization of the non-GPI anchored DRM marker, flotillin (Fig. S2 *A-C*). Furthermore, after PI-PLC treatment, hippocampal α_2-3 and δ-3 were both lost from the detergent phase and recovered in the aqueous phase after temperature-induced phase separation in Triton X-114 (Fig. 1*F*, star), as described for other GPI-anchored proteins (13). Parallel blots for flotillin showed that the phase distribution of this protein, which is associated with DRMs by virtue of its myristoylation and palmitoylation (18), was not affected by PI-PLC. A similar result was obtained with trypanosomal GPI-PLC (Fig. S2*D*).

A generally accepted proof that a protein contains a GPI anchor is the presence of the cross reacting determinant (CRD) epitope (13), an antigenic carbohydrate determinant, including inositol 1, 2-cyclic phosphate, which is created after PI-PLC cleavage (19). In the aqueous phase after PI-PLC treatment, CRD immunoreactivity was associated with a band of the same mobility as PI-PLC-treated deglycosylated hippocampal δ-3 (Fig. 1*F*, arrow). This band at 17 kDa was absent when the sample was examined under nonreducing conditions and free δ-3 would not be formed (Fig. S2*E*).

To examine whether or not acute PI-PLC treatment would affect the properties of calcium-channel currents including $\alpha_2\delta$-3, we incubated tsA-201 cells expressing $Ca_V2.2/\alpha_2\delta$-3/β1b with PI-PLC for 90 min and found this reduced peak I_{Ba} by 60.7 ± 9.7% (Fig. 1*G*). This reduction agrees with the observation that these channels are less stable at the plasma membrane in the absence of $\alpha_2\delta$ (20). In contrast, in the absence of coexpressed $\alpha_2\delta$, there was no inhibition of $Ca_V2.2/\beta1b$ currents by PI-PLC treatment (Fig. 1*H*).

Effect of Mutation of the $\alpha_2\delta$-3 Predicted GPI-Anchor Motifs. GPI-anchoring motifs have no fixed sequence, but the ω-residues are usually small and polar and ω+2 is usually Gly, Ala, or Ser (Fig. 1*A*) (13). We mutated residues in the amino acid motif (CGGAS), which spans the two predicted ω-sites of $\alpha_2\delta$-3 (Fig. 1*A*), to large hydrophobic or charged residues (WKW) that were poorly predicted to support GPI modification. We found that, although the mutant $\alpha_2\delta$-3 proteins were well expressed in the whole-cell lysate (WCL), they were poorly delivered to DRMs (Fig. 2*A*).

We next compared the ability of $\alpha_2\delta$-3 and the two $\alpha_2\delta$-3 GPI-site mutants to enhance calcium-channel currents. We observed that, whereas wild-type (WT) $\alpha_2\delta$-3 enhanced the peak $Ca_V2.2/\beta1b$ I_{Ba} by about 4.5-fold, the CGG-WKW mutant reduced the peak I_{Ba} compared with currents in the absence of $\alpha_2\delta$ (Fig. 2 *B* and *C*). A potential explanation of the reduction is that the mutant induces intracellular retention of the α1 subunit, which we suggested previously for Von Willebrand Factor A domain mutants of $\alpha_2\delta$-2 (21). In contrast, the GAS-WKW $\alpha_2\delta$-3 still produced a small increase in I_{Ba} and indeed, is still predicted to be a substrate, albeit a poor one, for GPI modification.

In agreement with these functional results, we found that the GPI mutant $\alpha_2\delta$-3 proteins, particularly the CGG-WKW mutant, showed only low expression on the plasma membrane, which was judged by cell-surface biotinylation (Fig. 2 *D* and *E*); this cor-

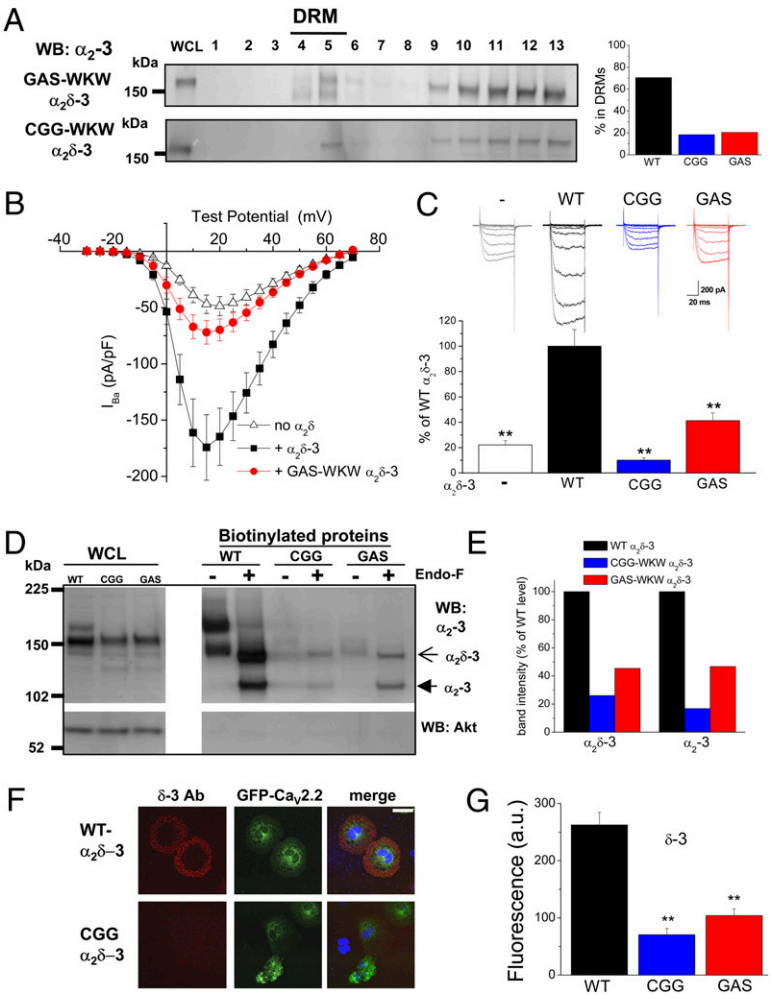

Fig. 2. Evidence that GPI-anchoring of $\alpha_2\delta$-3 is required for cell-surface localization and function. *(A Left)* Immunoblot profile of GAS-WKW $\alpha_2\delta$-3 (*Upper*) and CGG-WKW $\alpha_2\delta$-3 (*Lower*) in DRM fractions from transfected tsA-201 cells using α_2-3 (71–90) Ab. (*Right*) Bar chart showing the average proportion of the total $\alpha_2\delta$-3 found to be in DRM (sucrose gradient fractions 4–6) for WT $\alpha_2\delta$-3 (black bar), CGG-WKW $\alpha_2\delta$-3 (blue bar), and GAS-WKW $\alpha_2\delta$-3 (red bar) from two independent experiments each. (*B*) Mean *I-V* relationship for $Ca_V2.2/\beta1b$ coexpressed with WT $\alpha_2\delta$-3 (■; n = 12), with GAS-WKW $\alpha_2\delta$-3 (red ●; n = 25), or without $\alpha_2\delta$ (△; n = 23) in tsA-201 cells. All recordings are in 5 mM Ba^{2+}. (*C*) Peak I_{Ba} (mean ± SEM) measured at +15 mV was determined from *I-V* relationships including those in *A*. $Ca_V2.2/\beta1b$ is shown without $\alpha_2\delta$ (white bar; n = 36), with WT $\alpha_2\delta$-3 (black bar; n = 16), with CGG-WKW $\alpha_2\delta$-3 (blue bar; n = 22), or with GAS-WKW $\alpha_2\delta$-3 (red bar; n = 25). Data were pooled from several experiments and normalized to the respective control (+WT $\alpha_2\delta$-3) in each experiment. The statistical significances of the differences compared to +WT $\alpha_2\delta$-3 were determined by ANOVA and post hoc Bonferroni test. **, $P < 0.001$. Example I_{Ba} currents (from −30 mV to +15 mV from a holding potential of −90 mV) are shown above the bars for no $\alpha_2\delta$ (gray), WT $\alpha_2\delta$-3 (black), CGG-WKW $\alpha_2\delta$-3 (blue), and GAS-WKW $\alpha_2\delta$-3 (red). (*D Upper*) Cell-surface biotinylation of $\alpha_2\delta$-3 (WT), CGG-WKW $\alpha_2\delta$-3 and GAS-WKW $\alpha_2\delta$-3. The left three lanes show WCL, and the right six lanes show WT and mutant $\alpha_2\delta$-3 after cell-surface biotinylation, before and after deglycosylation with EndoF as indicated. Open arrow, full-length $\alpha_2\delta$-3; closed arrow, cleaved α_2-3. *Lower* shows lack of biotinylation of cytoplasmic Akt. (*E*) Quantification of relative amounts of full-length $\alpha_2\delta$-3 and cleaved α_2-3 for the CGG-WKW $\alpha_2\delta$-3 (blue) and GAS-WKW $\alpha_2\delta$-3 (red) mutants at the cell surface from two experiments, including the data shown in *C*, that were normalized to the amount in the WCL. (*F*) Confocal microscopic images showing membrane localization of $\alpha_2\delta$-3 using the δ-3 Ab (*Left*, red) for WT (*Upper*) and CGG-WKW $\alpha_2\delta$-3 (*Lower*) when coexpressed with green fluorescent protein $Ca_V2.2$ (*Middle*) and β1b in nonpermeabilized Cos-7 cells. (*Right*) Merged images show nuclear staining with DAPI (blue). Note that cell-surface staining in nonpermeabilized Cos-7 cells is seen, not as a fine ring but as a wide annulus, because of the flattened geometry (see also Fig. S3*A*). (Scale bar: 50 μm on merged images.) (*G*) Quantification of cell-surface immunofluorescence using δ-3 Ab for WT $\alpha_2\delta$-3 (black bars; n = 68), CGG-WKW $\alpha_2\delta$-3 (blue bars; n = 38), and GAS-WKW $\alpha_2\delta$-3 (red bars; n = 38). Statistical significance is $P < 0.001$ for one-way ANOVA and Tukey's post hoc tests.

relates well with the relative effect of these mutants on $Ca_V2.2$ I_{Ba} (Fig. 2*C*). Furthermore, immunocytochemical imaging also revealed much less of the GPI-mutant $\alpha_2\delta$-3 constructs on the cell surface of transfected Cos-7 cells compared with WT $\alpha_2\delta$-3 using both the δ-3 Ab (Fig. 2 *F* and *G*) and the α_2-3 Ab (Fig. S3). However, there was similar total expression (Fig. S3*A*).

Biochemical and Functional Evidence that $\alpha_2\delta$-2 Is Anchored by GPI. We then examined whether or not $\alpha_2\delta$-2 subunits can also be anchored by GPI (Fig. 3*A*), because we had shown previously that the $\alpha_2\delta$-2 subunit was localized mainly in DRMs, both in native tissue and after heterologous expression (14). We found that in DRMs prepared from cells expressing $\alpha_2\delta$-2, an ∼18-kDa band representing deglycosylated WT δ-2 was recognized by two anti-peptide δ-2 Abs (1062-1079 and 1080-1094) (Fig. 3*B*). However, an Ab raised against the 15 C-terminal residues of δ-2 (1133-1147) did not recognize the ∼18-kDa deglycosylated δ-2 species (Fig. 3*B Left*, asterisk; see Fig. S4*A* for evidence that this Ab does recognize GPI-mutant $\alpha_2\delta$-2 where the C terminus is not cleaved). This indicated that the ∼18-kDa δ-2 protein does not contain the extreme C-terminal residues. Furthermore, we generated a C-terminal myc-tagged $\alpha_2\delta$-2 and expressed it in Cos-7 cells to find that the myc tag was cleaved from both cell surface-expressed (Fig. S4*B*) and PI-PLC–released $\alpha_2\delta$-2 (Fig. S4*C*). In light of our results with $\alpha_2\delta$-3, an obvious possibility for further C-terminal processing would be cleavage of the C terminus associated with the formation of a GPI anchor (Fig. 3*A*). We then showed that incubation with PI-PLC of $\alpha_2\delta$-2 in DRMs resulted in a characteristic increase of apparent MW of δ-2 and a decrease in immunoreactivity, which was observed with δ-3 (Fig. 3*C*). A similar shift after PI-PLC treatment was seen for δ-2 concentrated in DRMs from cerebellum (Fig. 3*D*), and this species was also not immunoreactive with the C-terminal δ-2 (1133-1147) Ab (Fig. 3*D*). PI-PLC–cleaved cerebellar $\alpha_2\delta$-2 also partitioned into the aqueous phase after Triton X-114 phase separation (Fig. S5*A*, asterisk).

To examine whether or not a CRD epitope was revealed on $\alpha_2\delta$-2 by PI-PLC treatment, we immunoprecipitated and concentrated $\alpha_2\delta$-2 from DRMs using an internal HA tag in α_2-2 (14) (Fig. 3*E*). As we have previously reported (14), the main species of HA-$\alpha_2\delta$-2 present in tsA-201 cells is uncleaved $\alpha_2\delta$-2, indicating that proteolytic cleavage into α_2 and δ is incomplete in heterologous-expression systems, unlike in native tissues. This is shown by the presence of both α_2 and δ immunoreactivity in the ∼190-kDa band (Fig. 3*E*). Importantly, only the PI-PLC–treated $\alpha_2\delta$-2 exhibited positive CRD immunoreactivity, and this was the case for both the glycosylated and deglycosylated $\alpha_2\delta$-2 (Fig. 3*F*). PI-PLC-treated 5′-nucleotidase (5′NT) was used as a positive-control GPI-anchored protein (Fig. S5*B*). A reduction in CRD immunoreactivity was seen on incubation of the deglycosylated PI-PLC-treated HA-$\alpha_2\delta$-2 with 1 M HCl to destroy the CRD epitope (Fig. S5*C*). The fact that CRD immunoreactivity was associated with the uncleaved $\alpha_2\delta$-2 band indicates that for-

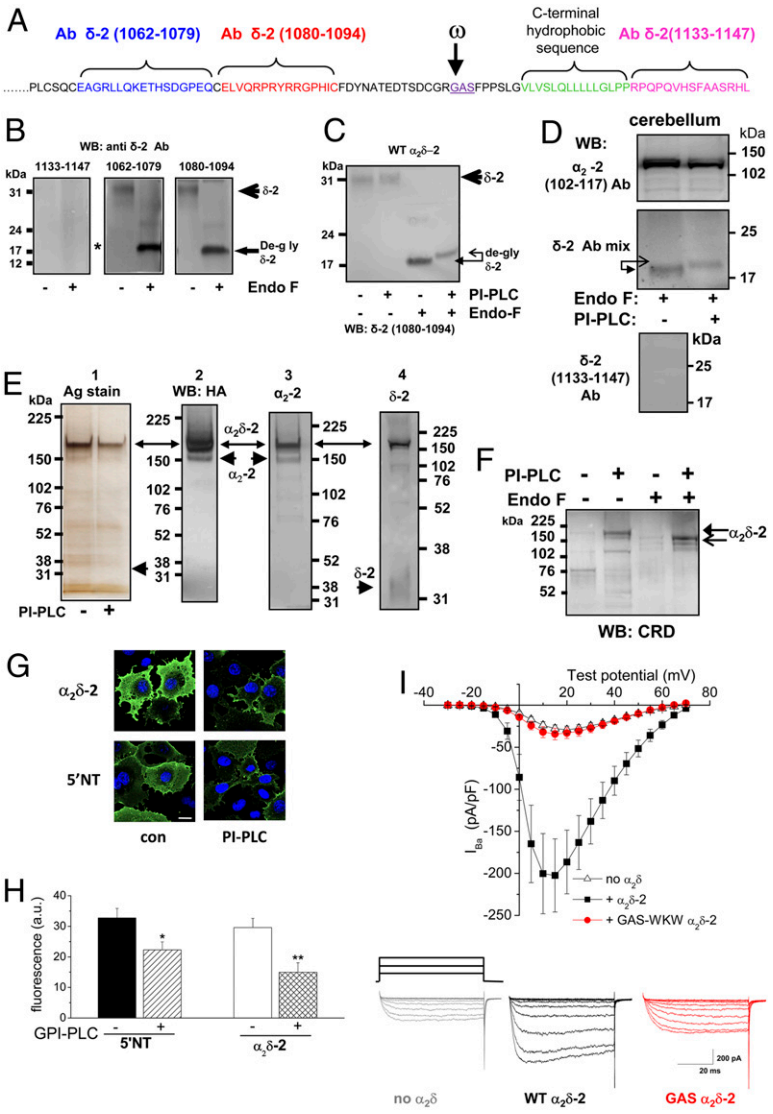

Fig. 3. Biochemical and functional evidence that $\alpha_2\delta$-2 is anchored by GPI. *(A)* Amino acid sequence of mouse $\alpha_2\delta$-2 C terminus showing the peptides used to generate the δ-2 (1062-1079), δ-2 (1080-1094), and δ-2 (1133-1147; C-terminus, CT) Abs in blue, red, and pink, respectively. The predicted GPI-anchor site (in purple and underlined with ω indicated by the arrow) and the C-terminal hydrophobic sequence (green) are also shown. (*B*) Immunoblot of δ-2 from peak DRM fractions prepared from an $\alpha_2\delta$-2 stable cell line (14), which shows the absence of immunoreactivity to the C-terminal δ-2 (1133-1147) Ab (*Left*; see Fig. S4*A* for validation of this Ab) but immunoreactivity to other δ-2 Abs (1062-1079; *Center*) and (1080-1094; *Right*). (*C*) Immunoblot of δ-2 from the peak DRM fraction derived from $\alpha_2\delta$-2–expressing tsA-201 cells before and after incubation with PI-PLC and subsequent deglycosylation with EndoF as indicated. The Ab used was δ-2 (1080-1094). The arrows show the upward shift of the δ-2 protein after PI-PLC. (*D Top*) Immunoblot of α_2-2 from the peak DRM fraction derived from cerebellum before and after incubation with PI-PLC as indicated and subsequent deglycosylation with EndoF. (*Middle*) Immunoblot of δ-2 from the same fractions. A mixture of all anti–δ-2 Abs was used for this immunoblot. The arrows show the upward shift of the δ-2 protein after PI-PLC. (*Bottom*) Immunoblot of δ-2 with the δ-2 (1133-1147; CT) Ab alone from the same fractions before PI-PLC treatment, which shows the absence of immunoreactivity. (*E*) Immunoprecipitated HA-tagged $\alpha_2\delta$-2 treated or not treated with PI-PLC before purification is indicated in panel 1. Silver-stained gel was used for the affinity-purified HA-tagged $\alpha_2\delta$-2; full-length $\alpha_2\delta$-2 is the main species purified by this procedure, possibly because of the greater accessibility of the HA tag. These data also confirm that the PI-PLC used does not have any significant proteolytic activity, because no proteolytic fragments of $\alpha_2\delta$-2 were observed after 3 h of incubation. Panel 2 shows corresponding anti-HA blot; panel 3 shows blot for α_2-2 with α_2-2 (102-117) Ab. Panels 1–3 used 3–8% Tris acetate gel. Panel 4 shows the blot for δ-2 with δ-2 (1080-1094) Ab using a 12% Bis-Tris gel for better resolution of δ-2. Arrows indicate the position of $\alpha_2\delta$-2, and arrowheads show α_2-2 and δ-2. The material shown in panel 1 was then adjusted to equal protein concentration before immunoblotting for CRD. (*F*) Immunoblot with anti-CRD Ab. Lane 1 shows $\alpha_2\delta$-2 without PI-PLC treatment. Lane 2 shows $\alpha_2\delta$-2 after PI-PLC treatment. Lane 3 shows deglycosylated $\alpha_2\delta$-2 without PI-PLC treatment. Lane 4 shows deglycosylated $\alpha_2\delta$-2 after PI-PLC treatment that showed an ∼170-kDa band corresponding to HA-a$_2\delta$-2 and a 150-kDa band corresponding to deglycosylated HA–$\alpha_2\delta$-2 (arrows). The CRD antibody has a low affinity, and we were unable to examine immunoreactivity against a band corresponding to free δ-2, because very little was purified using the internal HA tag in α_2-2 (see silver-stained gel and δ-2 blot in *E*). (*G*) Effect of acute incubation of Cos-7 cells for 1 h with PI-PLC (4 U/mL) on cell-surface localization of transfected 5′NT and $\alpha_2\delta$-2. Representative confocal microscopic images of $\alpha_2\delta$-2 (102-117 Ab; *Upper*) and 5′NT (*Lower*) cell-surface expression in transfected nonpermeabilized COS-7 cells (nuclei visualized with DAPI) were treated with either vehicle (con, left) or PI-PLC (right). (Scale bar: 20 μm.) (*H*) Quantification of immunofluorescence data similar to those shown in *G* were obtained from epifluorescence images for 5′NT incubated with vehicle (black bar; $n = 25$) or PI-PLC (Glyko; hatched bar; $n = 31$) and for $\alpha_2\delta$-2 incubated with vehicle (white bar; $n = 30$) or PI-PLC (cross-hatched bar; $n = 20$). The statistical significances of the differences with and without PI-PLC treatment were determined by Student's *t* test. *, $P = 0.0083$ for 5′NT; **, $P = 0.0019$ for $\alpha_2\delta$-2. (*I Upper*) Mean *I-V* relationship for $Ca_V2.2/\beta1b$ coexpressed with $\alpha_2\delta$-2 (■ $n = 12$), with $\alpha_2\delta$-2 GAS-WKW (red ● $n = 24$), or without $\alpha_2\delta$ (△; $n = 18$) in tsA-201 cells. All recordings are in 5 mM Ba^{2+}. (*Lower*) Example I_{Ba} currents (from −30 mV to +15 mV from a holding potential of −90 mV) are shown for no $\alpha_2\delta$ (gray), $\alpha_2\delta$-2 (black), and GAS-WKW $\alpha_2\delta$-2 (red).

mation of the GPI anchor occurs before proteolysis into α_2-2 and δ-2. Furthermore, incubation of the HA-$\alpha_2\delta$-2 cell line with [^{3}H]-inositol resulted in incorporation of [^{3}H] into a band at the level of HA-$\alpha_2\delta$-2 (Fig. S6).

As further confirmation that $\alpha_2\delta$-2 is associated with the plasma membrane by a GPI anchor, we found that acute incubation of Cos-7 cells for 1 h with PI-PLC significantly reduced the amount of cell-surface expression, both of 5′NT by 31.9% and of expressed $\alpha_2\delta$-2 by 49.4% (Fig. 3 *G* and *H*). Similar results were found for $\alpha_2\delta$-3 (33.9 ± 5.5% reduction; $n > 100$ cells examined in each condition). Importantly, in the same system, there was no effect of a high concentration of PI-PLC (8 U/mL) on cell-surface expression of a known transmembrane protein (α7 nicotinic cholinergic receptor per 5HT3 receptor chimera; Fig. S7).

Mutational Evidence that $\alpha_2\delta$-2 Is Anchored by GPI. Next, we mutated the predicted GPI-anchor site in $\alpha_2\delta$-2 (GAS to WKW, Fig. 3*A*). An ∼23-kDa deglycosylated band, the correct MW to represent a mutant δ-2 species retaining the C terminus, was recognized by both the δ-2 (1080-1094) Ab and the C-terminal δ-2 (1133-1147) Ab (Fig. S4*A*). However, no ∼18-kDa δ-2 band was present, suggesting that GAS-WKW $\alpha_2\delta$-2 was not C-terminally truncated, unlike WT $\alpha_2\delta$-2 (Fig. 3*B*; Fig. S4*A*). Like the $\alpha_2\delta$-3 GPI mutants, the $\alpha_2\delta$-2 GPI mutant also showed a reduction in its ability to partition into DRMs (Fig. S8*A*). GAS-WKW $\alpha_2\delta$-2 also showed a reduction in expression on the plasma membrane, which was determined by cell-surface biotinylation (30.7% of WT $\alpha_2\delta$-2 for the α_2-2 protein; Fig. S8*B*). We then examined its functionality and found that the GAS-WKW $\alpha_2\delta$-2 was unable to enhance $Ca_V2.2$ I_{Ba} compared with the currents observed in the absence of $\alpha_2\delta$ (Fig. 3*I*).

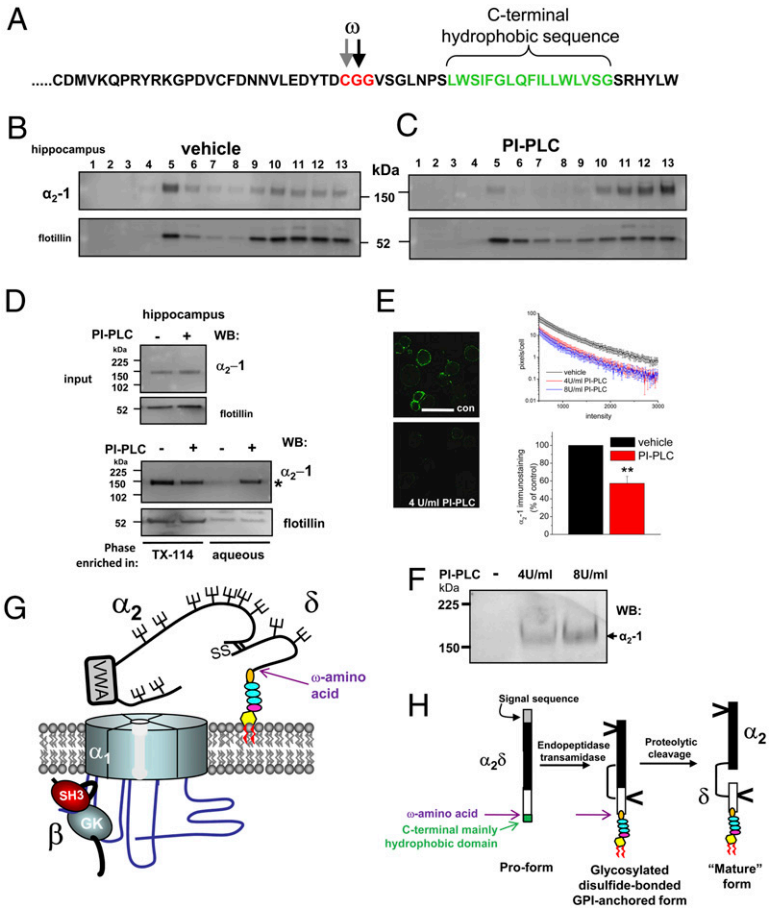

Fig. 4. Evidence that GPI anchoring of $\alpha_2\delta$-1 is required for cell-surface localization and function. *(A)* Amino acid sequence of rat $\alpha_2\delta$-1 C terminus showing the predicted GPI-anchor sites (ω) and the C-terminal hydrophobic sequence (green). (*B* and *C*) Lysates from the hippocampus were incubated with vehicle (*B*) or PI-PLC (*C*) at 37°C in the presence of protease inhibitors, and then they were subjected to sucrose gradient centrifugation. (*Upper*) The immunoblot profile of $\alpha_2\delta$-1 in DRMs from hippocampus is shown using the α_2-1 monoclonal Ab. (*Lower*) Flotillin distribution in same DRM profile. (*D*) Phase separation of α_2-1 after PI-PLC treatment. (*Upper*) Peak DRM fraction before phase separation showing input for α_2-1 and flotillin. (*Lower*) Phase separation after vehicle or PI-PLC treatment and Triton X-114 extraction shows α_2-1 in aqueous phase after PI-PLC (indicated by asterisk). Flotillin was not redistributed into the aqueous phase after PI-PLC treatment. (*E Left*) Immunolocalization of $\alpha_2\delta$-1 in non-permeabilized DRG neurons after 2 days in culture after incubation with vehicle (*Upper*; confocal field contains 12 DRG neurons) or with 4 U/mL PI-PLC for 60 min (*Lower*; field contains 10 DRG neurons). (Scale bar: 50 μm.) (*Right*) Quantification of $\alpha_2\delta$-1 immunostaining expressed as number of pixels per cell ($\log_{10}$ scale) in the intensity range 500-3,000 for 18 images from three different coverslips for each condition, each containing between 5 and 12 cells (*Upper*). Black line, vehicle-treated; red line, 4 U/mL PI-PLC; blue line, 8 U/mL PI-PLC. (*Lower*) Quantification of immunostaining in four separate experiments after vehicle (black bar; normalized to 100%) relative to PI-PLC (4 U/mL or 8 U/mL; red bar). **, $P < 0.001$ for Student's *t* test. (*F*) Immunoblot of supernatant after PI-PLC treatment of DRGs, as in *E*, for 4 U/mL and 8 U/mL PI-PLC. The arrow shows the presence of α_2-1. (*G*) Cartoon showing the structure of $\alpha_2\delta$ subunits that is identified here. The GPI anchor consists of ethanolamine (orange), three mannose rings (blue), glucosamine (pink), and inositol (yellow). (*H*) Proposed scheme for processing $\alpha_2\delta$ proteins. The N-terminal signal sequence is in gray, the C-terminal GPI signal sequence is in green, the α_2 sequence is in black, and the δ sequence is in white. The GPI anchor is drawn as in *G*. The position of the ω amino acid is indicated by a purple arrow in *G* and *H*.

Biochemical and Functional Evidence that $\alpha_2\delta$-1 Is Anchored by GPI. Finally, we also obtained evidence that $\alpha_2\delta$-1 is anchored by GPI as predicted from its C-terminal sequence (Fig. 4*A*). Both heterologously expressed $\alpha_2\delta$-1 (Fig. S8*C*), and native $\alpha_2\delta$-1 from hippocampus and cardiac muscle partition strongly into DRMs (Fig. 4*B* for hippocampus). Furthermore, PI-PLC treatment of hippocampal lysates reduced the DRM association of $\alpha_2\delta$-1 from 68.3 ± 8.0% to 8.3 ± 4.6% ($P = 0.0034$ from three independent experiments, including the experiment in Fig. 4*C*), and also resulted in recovery of α_2-1 in the aqueous phase after Triton X-114 separation (Fig. 4*D*, asterisk).

Dorsal root-ganglion neurons (DRGs) represent a heterogeneous class of sensory neurons that express $\alpha_2\delta$-1 on their cell surface (22). We found that $\alpha_2\delta$-1 is also well expressed on the plasma membrane of DRGs in culture (Fig. 4*E*) and that incubation of cultured DRGs for 60 min with PI-PLC substantially reduced cell-surface $\alpha_2\delta$-1 immunofluorescence (Fig. 4*E*). However, it did not reduce that for the transmembrane p75 nerve growth-factor receptor (Fig. S9). In the same experiments, PI-PLC treatment of cultured DRGs also resulted in the appearance of $\alpha_2\delta$-1 in the supernatant, showing that it had been shed from the cell surface (Fig. 4*F*).

Discussion

Taken together, these results provide evidence that all of the $\alpha_2\delta$ subunits studied (isoforms 1–3) are able to form GPI-anchored proteins (Fig. 4*G*). The $\alpha_2\delta$-4 subunit is also strongly predicted to be anchored by GPI. Although all $\alpha_2\delta$ subunits have a C-terminal hydrophobic domain, which led to the original description of $\alpha_2\delta$-1 as a type-I single-pass transmembrane protein (4–8), GPI-anchored proteins also require a C-terminal hydrophobic sequence. In addition, they usually have little or no cytoplasmic domain, features exhibited by the $\alpha_2\delta$ proteins. They frequently have one or more prolines in or near the C-terminal hydrophobic domains (23), which is also the case for the $\alpha_2\delta$ subunits. Whereas $\alpha_2\delta$-2 has the longest predicted C-terminal cytoplasmic domain of the $\alpha_2\delta$ subunits (~15 residues), there are other key determinants within the C-terminal domain that dictate GPI anchoring, even in the presence of a hydrophilic C-terminal extension (23, 24). Our results also indicate that GPI-anchoring occurs before proteolytic cleavage into α_2 and δ (Fig. 4*H*). Nevertheless, from the present results, we cannot rule out the coexistence of transmembrane forms of $\alpha_2\delta$ subunits, and such alternative processing has been shown for other GPI-anchored proteins (25). However, an $\alpha_2\delta$-1 chimera containing the transmembrane segment of adhalin was previously found to be unable to enhance calcium currents (8).

As a consequence of the GPI-anchored structural form of $\alpha_2\delta$ subunits revealed here, the reported role of the transmembrane segments of δ subunits to influence the biophysical properties of calcium channels (8, 10) and the limited structural information on calcium-channel complexes (26, 27) may require reinterpretation. Some important implications of GPI anchoring of $\alpha_2\delta$ subunits include that they may direct the localization of interacting partners, including $Ca_V\alpha1$ subunits, into specific DRM domains. Indeed, we have shown that a population of $Ca_V2.1$ is present in DRMs prepared from the cerebellum (14). Calcium-channel complexes or $\alpha_2\delta$ subunits playing other roles [e.g., in synapse formation (28, 29)] may participate in nanodomain signaling complexes, and thrombospondin is one identified interacting partner (28). Additionally, modification of lipid-raft composition by acute cholesterol depletion has marked effects on calcium-channel currents (14). Also, it opens the possibility that $\alpha_2\delta$ subunits could be dynamically shed from the plasma membrane by the

action of native extracellular PI-PLC enzymes (30). Therefore, it could acutely alter calcium-channel function or other functions of $\alpha_2\delta$ proteins (28, 29) that may involve soluble forms of $\alpha_2\delta$ (29). For $\alpha_2\delta$-1, this would be particularly relevant at presynaptic terminals where it is concentrated (22, 31). In relation to this, the $\alpha_2\delta$-1 protein is up-regulated in DRG neurons in neuropathic pain (22), and it is the main therapeutic target for gabapentinoid drugs in the alleviation of this condition (32, 33).

Materials and Methods

Standard molecular biological, biochemical, and electrophysiological techniques were used as described previously (14, 21, 33) and in *SI Materials and Methods*. Details of all Abs used are also provided in *SI Materials and Methods*. Where data are given as mean ± SEM, statistical comparisons were performed using either Student's *t* test or ANOVA with a post hoc test, as appropriate.

ACKNOWLEDGMENTS. We thank Prof. N. Hooper (Leeds University) for advice and reagents (CRD Ab), Dr. L.F. Thompson (Oklahoma Medical Research Foundation) for 5′NT cDNA, Dr. M. Carrington (Cambridge University) for GPI-PLC, Prof. N. Millar (University College London) for α7 nicotinic receptor/5HT3 chimera, A. Tran-Van-Minh for advice, and K. Chaggar for technical support. We thank the Medical Research Council (UK), Biotechnology and Biological Sciences Research Council (UK), Wellcome Trust, and Epilepsy Research UK for support. A.A.-L. is a Biotechnology and Biological Sciences Research Council (UK) PhD student.

1. Flockerzi V, et al. (1986) Purified dihydropyridine-binding site from skeletal muscle t-tubules is a functional calcium channel. *Nature* 323:66–68.
2. Takahashi M, Seagar MJ, Jones JF, Reber BFX, Catterall WA (1987) Subunit structure of dihydropyridine-sensitive calcium channels from skeletal muscle. *Proc Natl Acad Sci USA* 84:5478–5482.
3. Catterall WA (2000) Structure and regulation of voltage-gated Ca^{2+} channels. *Annu Rev Cell Dev Biol* 16:521–555.
4. Ellis SB, et al. (1988) Sequence and expression of mRNAs encoding the α_1 and α_2 subunits of a DHP-sensitive calcium channel. *Science* 241:1661–1664.
5. De Jongh KS, Warner C, Catterall WA (1990) Subunits of purified calcium channels. α 2 and δ are encoded by the same gene. *J Biol Chem* 265:14738–14741.
6. Jay SD, et al. (1991) Structural characterization of the dihydropyridine-sensitive calcium channel α_2-subunit and the associated δ peptides. *J Biol Chem* 266:3287–3293.
7. Brickley K, et al. (1995) Use of site-directed antibodies to probe the topography of the α 2 subunit of voltage-gated Ca^{2+} channels. *FEBS Lett* 364:129–133.
8. Gurnett CA, De Waard M, Campbell KP (1996) Dual function of the voltage-dependent Ca^{2+} channel $\alpha_2\delta$ subunit in current stimulation and subunit interaction. *Neuron* 16:431–440.
9. Klugbauer N, Marais E, Hofmann F (2003) Calcium channel alpha2delta subunits: Differential expression, function, and drug binding. *J Bioenerg Biomembr* 35:639–647.
10. Felix R, Gurnett CA, De Waard M, Campbell KP (1997) Dissection of functional domains of the voltage-dependent Ca2+ channel alpha2delta subunit. *J Neurosci* 17:6884–6891.
11. Davies A, et al. (2007) Functional biology of the alpha(2)delta subunits of voltage-gated calcium channels. *Trends Pharmacol Sci* 28:220–228.
12. Fankhauser N, Mäser P (2005) Identification of GPI anchor attachment signals by a Kohonen self-organizing map. *Bioinformatics* 21:1846–1852.
13. Hooper NM (2001) Determination of glycosyl-phosphatidylinositol membrane protein anchorage. *Proteomics* 1:748–755.
14. Davies A, et al. (2006) The calcium channel α2δ-2 subunit partitions with CaV2.1 into lipid rafts in cerebellum: Implications for localization and function. *J Neurosci* 26:8748–8757.
15. Bütikofer P, Malherbe T, Boschung M, Roditi I (2001) GPI-anchored proteins: Now you see 'em, now you don't. *FASEB J* 15:545–548.
16. Barboni E, et al. (1995) The glycophosphatidylinositol anchor affects the conformation of Thy-1 protein. *J Cell Sci* 108:487–497.
17. Elfrink K, et al. (2008) Structural changes of membrane-anchored native PrP(C). *Proc Natl Acad Sci USA* 105:10815–10819.
18. Langhorst MF, Reuter A, Stuermer CA (2005) Scaffolding microdomains and beyond: The function of reggie/flotillin proteins. *Cell Mol Life Sci* 62:2228–2240.
19. Bordier C, Etges RJ, Ward J, Turner MJ, Cardoso de Almeida ML (1986) Leishmania and Trypanosoma surface glycoproteins have a common glycophospholipid membrane anchor. *Proc Natl Acad Sci USA* 83:5988–5991.
20. Bernstein GM, Jones OT (2007) Kinetics of internalization and degradation of N-type voltage-gated calcium channels: Role of the alpha2/delta subunit. *Cell Calcium* 41:27–40.
21. Cantí C, et al. (2005) The metal-ion-dependent adhesion site in the Von Willebrand factor-A domain of alpha2delta subunits is key to trafficking voltage-gated Ca2+ channels. *Proc Natl Acad Sci USA* 102:11230–11235.
22. Bauer CS, et al. (2009) The increased trafficking of the calcium channel subunit α2δ-1 to presynaptic terminals in neuropathic pain is inhibited by the α2δ ligand pregabalin. *J Neurosci* 29:4076–4088.
23. Dalley JA, Bulleid NJ (2003) The endoplasmic reticulum (ER) translocon can differentiate between hydrophobic sequences allowing signals for glycosylphosphatidylinositol anchor addition to be fully translocated into the ER lumen. *J Biol Chem* 278:51749–51757.
24. Watanabe K, et al. (2008) Characterization of the glycosylphosphatidylinositol-anchor signal sequence of human Cryptic with a hydrophilic extension. *Biochim Biophys Acta* 1778:2671–2681.
25. Dustin ML, Selvaraj P, Mattaliano RJ, Springer TA (1987) Anchoring mechanisms for LFA-3 cell adhesion glycoprotein at membrane surface. *Nature* 329:846–848.
26. Wolf M, Eberhart A, Glossmann H, Striessnig J, Grigorieff N (2003) Visualization of the domain structure of an L-type Ca2+ channel using electron cryo-microscopy. *J Mol Biol* 332:171–182.
27. Wang M-C, et al. (2004) The three-dimensional structure of the cardiac L-type voltage-gated calcium channel: Comparison with the skeletal muscle form reveals a common architectural motif. *J Biol Chem* 279:7159–7168.
28. Eroglu C, et al. (2009) Gabapentin receptor alpha2delta-1 is a neuronal thrombospondin receptor responsible for excitatory CNS synaptogenesis. *Cell* 139:380–392.
29. Kurshan PT, Oztan A, Schwarz TL (2009) Presynaptic alpha(2)delta-3 is required for synaptic morphogenesis independent of its Ca(2+)-channel functions. *Nat Neurosci* 12:1415–1423.
30. Traister A, Shi W, Filmus J (2008) Mammalian Notum induces the release of glypicans and other GPI-anchored proteins from the cell surface. *Biochem J.* 410:503–511.
31. Taylor CP, Garrido R (2008) Immunostaining of rat brain, spinal cord, sensory neurons and skeletal muscle for calcium channel alpha2-delta (alpha2-delta) type 1 protein. *Neuroscience* 155:510–521.
32. Field MJ, et al. (2006) Identification of the α2-δ-1 subunit of voltage-dependent calcium channels as a molecular target for pain mediating the analgesic actions of pregabalin. *Proc Natl Acad Sci USA* 103:17537–17542.
33. Hendrich J, et al. (2008) Pharmacological disruption of calcium channel trafficking by the α2δ ligand gabapentin. *Proc Natl Acad Sci USA* 105:3628–3633.